Growth, spectroscopy and first laser operation of monoclinic Ho^{3+}:$MgWO_4$ crystal

Lizhen Zhang[a], Pavel Loiko[b], Josep Maria Serres[c], Esrom Kifle[c], Haifeng Lin[a], Ge Zhang[a], Elena Vilejshikova[d], Elena Dunina[e], Alexey Kornienko[e], Liudmila Fomicheva[f], Uwe Griebner[g], Valentin Petrov[g], Zhoubin Lin[a], Weidong Chen[a,**], Kirill Subbotin[h], Magdalena Aguiló[c], Francesc Díaz[c], and Xavier Mateos[c,*]

[a]*Key Laboratory of Optoelectronic Materials Chemistry and Physics, Fujian Institute of Research on the Structure of Matter, Chinese Academy of Sciences, Fuzhou, 350002 Fujian, China,* [**]*chenweidong@fjirsm.ac.cn*
[b]*ITMO University, 49 Kronverkskiy Pr., 197101 St. Petersburg, Russia*
[c]*Universitat Rovira i Virgili, Departament Química Física i Inorgànica, Física i Cristal·lografia de Materials i Nanomaterials (FiCMA-FiCNA)-EMaS, Campus Sescelades, E-43007, Tarragona, Spain*
[d]*Center for Optical Materials and Technologies (COMT), Belarusian National Technical University, 65/17 Nezavisimosti Ave., 220013 Minsk, Belarus*
[e]*Vitebsk State Technological University, 72 Moskovskaya Ave., 210035 Vitebsk, Belarus*
[f]*Belarusian State University of Informatics and Radioelectronics, 6 Brovki St., 220027 Minsk, Belarus*
[g]*Max Born Institute for Nonlinear Optics and Short Pulse Spectroscopy, 2A Max-Born-Str., D-12489 Berlin, Germany*
[h]*Prokhorov General Physics Institute, Russian Academy of Sciences, 38 Vavilov St., 119991 Moscow, Russia*
**Corresponding author e-mail*: *xavier.mateos@urv.cat*

ABSTRACT. A monoclinic 0.86 at.% Ho^{3+}:$MgWO_4$ crystal is grown by the Top-Seeded-Solution Growth method. Its spectroscopic properties are studied with polarized light for $\boldsymbol{E} \parallel \boldsymbol{a}, \boldsymbol{b}, \boldsymbol{c}$. The Ho^{3+} ion transition probabilities are determined within the modified Judd-Ofelt theory (mJ-O) accounting for the configuration interaction. The intensity parameters are Ω_2 = 21.09, Ω_4 = 4.42, Ω_6 = 2.28 [10^{-20} cm^2] and α = 0.053 [10^{-4} cm]. The calculated radiative lifetime of the $^5I_7$ state is 6.18 ms. The Stark splitting of the $^5I_7$ and $^5I_8$ multiplets is determined with low-temperature spectroscopy. The absorption, stimulated-emission (SE) and gain cross-sections for the $^5I_8 \leftrightarrow {}^5I_7$ transition are derived. Ho^{3+}:$MgWO_4$ features a large Stark splitting of the ground-state (380 cm^{-1}), high maximum σ_{SE} of 1.82×10^{-20} cm^2 at 2.083 μm, broad gain spectra and high luminescence quantum yield making it suitable for efficient continuous-wave and mode-locked lasers at ~2.1 μm. First laser operation of Ho^{3+}:$MgWO_4$ crystal is demonstrated at 2.104 μm reaching a slope efficiency of 72%.

Keywords: Double tungstates; Holmium ions; Luminescence; Judd-Ofelt theory; Laser operation.

1. Introduction

The Holmium ion (Ho^{3+}) with an electronic configuration of $[Xe]4f^{10}$ exhibits eye-safe emission above 2 μm due to the transition from the first excited-state ($^5I_7$) to the ground-state ($^5I_8$) [1]. The Stark splitting of the latter multiplet is typically large (from 314 cm^{-1} for Ho^{3+}:$LiYF_4$ to 540 cm^{-1} for Ho^{3+}:$Y_3Al_5O_{12}$) [2,3] and determines the width of this emission band. The emission at >2 μm matches the absorption of water molecules (H_2O) in bio-tissues and in the atmosphere, so that Ho lasers are used for remote sensing, wind mapping [4,5] and in laser surgery. The Ho emission is also suitable for pumping mid-IR optical parametric oscillators (OPOs) and optical parametric amplifiers (OPAs) [6]. It is of great interest to develop novel Ho^{3+}-doped materials for continuous-wave (CW) and mode-locked (ML) bulk and thin-disk lasers at 2 μm, featuring high transition cross-sections with polarized light and broad emission properties.

Monoclinic (space group $C^4_{2h} – P2/c$) crystals of magnesium monotungstate ($MgWO_4$) doped with thulium (Tm^{3+}) ions have recently attracted a lot of attention for the development of CW and ML oscillators at 2 μm [7-9]. Such crystals belong to the family of monoclinic divalent-metal monotungstates $M^{2+}WO_4$ where M = Mg, Cu, Ni, Co, Fe, Zn, Mn or Cd [10-12]. As a host material, $MgWO_4$, is characterized by a relatively high thermal conductivity κ of ~8.7 W/mK measured for an arbitrary crystal orientation [13]. This value is higher than for the well-known monoclinic double tungstates (MDTs), e.g., $KLu(WO_4)_2$, for which κ is only ~3 W/mK [14]. Previous research on Tm-doping revealed that Tm^{3+} ions in $MgWO_4$ replace the Mg^{2+} ones in C_2 sites and the significant difference in their ionic radii, as well as the low site symmetry promote the broadening of the absorption and emission bands [7,15].

Efficient CW, Q-switched and ML Tm^{3+}:$MgWO_4$ lasers have been recently demonstrated [7-9]. In Ref. [8], a diode-pumped Tm^{3+}:$MgWO_4$ laser generated 3.09 W at 2022-2034 nm with a slope efficiency of 50%. A Ti:Sapphire pumped Tm^{3+}:$MgWO_4$ laser ML by a graphene saturable absorber generated 86 fs pulses at 2017 nm at a repetition rate of 87 MHz (emission bandwidth: 53 nm) [9], the shortest pulses achieved with a bulk ML crystalline laser at ~2 μm. Very recently, we analyzed spectroscopically a unique feature of Tm^{3+}:$MgWO_4$ to generate linearly polarized broadband emission above 2 μm [15].

Compared to Tm^{3+}, the Ho^{3+} ion provides longer emission wavelength and higher laser slope efficiency. The latter is realized by employing the so-called resonant (in-band) pumping directly to the upper laser level ($^5I_7$) [16,17]. In this case, a slope efficiency approaching the Stokes efficiency, e.g., >80%, is feasible [18]. The weak heat loading diminishes the thermo-optic effects. $MgWO_4$ crystals doped with Ho^{3+} ions have not been studied so far. Note that Ho^{3+}-doped MDTs, namely $KLu(WO_4)_2$, $KGd(WO_4)_2$ and $KY(WO_4)_2$, have been successfully used in bulk and thin-disk lasers [19,20].

In the present work, we aimed to grow a Ho:$MgWO_4$ crystal, to perform a detailed room- and low-temperature spectroscopic characterization and to demonstrate the first laser operation of this monoclinic crystal.

2. Crystal growth

The Ho^{3+}:$MgWO_4$ crystal was grown by the Top Seeded Solution Growth (TSSG) method (from the flux, with sodium tungstate, Na_2WO_4, as a solvent). The reagents used were MgO,

WO_3, Na_2CO_3 (AR-grade purity) and Ho_2O_3 (99.99% purity). The ratio of $MgWO_4$: Na_2WO_4 in the melt was 5:7 (mol). The stoichiometric amounts of raw materials with 10 at.% Ho_2O_3 were mixed and melted in a platinum crucible. Then the melt was heated to 970 °C and held for 48 hours to make the solution homogeneous in a home-made vertical tubular furnace with a nickel-chrome wire as a heating element. When the saturation temperature (934 °C) of the solution was exactly determined, the crystal was grown at a cooling rate of 0.6-1 °C/day and rotated at a rate of 10 revolutions per minute (rpm). After a period of ~25 days, the crystal was pulled out of the solution and cooled to room temperature at a rate of 12 °C per hour.

A single crystal with dimensions of 20×8×8 mm^3 was obtained, as shown in Fig 1(a). The crystal was free of cracks and inclusions and it had a yellow-brown coloration.

3. Experimental

For room temperature (RT, 293 K) X-ray diffraction (XRD), we used a MiniFlex 600 powder diffractometer with Cu Kα radiation (λ = 0.154187 nm). The sample was finely powdered. High-temperature XRD patterns were recorded using a Siemens D5000 diffractometer equipped with an Anton-Paar HTK10 platinum ribbon heating stage.

The RT absorption spectra were measured using a Varian CARY 5000 spectrophotometer (spectral resolution: 0.1 nm) equipped with a Glan-Taylor polarizer.

The spectra of near-IR luminescence were measured using an Optical Spectrum Analyzer (OSA, Yokogawa, model AQ6375B). The luminescence was excited by a CW GaSb laser diode emitting at 1926 nm. The spectra of visible luminescence were measured using a Renishaw inVia confocal Raman microscope with a Leica ×50 objective. The excitation wavelength was 457 nm (an Ar^+ laser line). In both cases, a Glan-Taylor polarizer was used to control the polarization of Ho^{3+} luminescence.

The low-temperature (LT, 6 K) absorption and emission measurements were done using an Oxford Instruments Ltd. cryostat (model SU 12) with helium-gas close-cycle flow.

For the luminescence decay measurements, we used mechanically chopped output of the GaSb laser diode emitting at 1926 nm as an excitation source. To detect luminescence, we used OSA and a 2 GHz digital oscilloscope (Tektronix DPO5204B).

4. Crystal structure

4.1 Lattice constants

The X-ray powder diffraction pattern of the as-grown Ho^{3+}:$MgWO_4$ crystal recorded at RT is shown in Fig. 1(b). The measured XRD pattern is consistent with the standard pattern of undoped $MgWO_4$ (ICDD card #27-0789). The Ho^{3+}:$MgWO_4$ crystal is monoclinic (space group C^4_{2h} – *P*2/*c*, No. 13, centrosymmetric point group 2/*m*), the lattice constants are a = 4.6958(3) Å, b = 5.6822(3) Å, c = 4.9358(3) Å, $\alpha = \gamma = 90^o$, $\beta = \boldsymbol{a}\hat{}\boldsymbol{c} = 90.744(4)^o$, the volume of the unit cell V = 131.69(2) $Å^3$. The calculated crystal density is ρ_{calc} = 6.863 g/cm^3 (the number of the formula units in the unit-cell Z = 2). The determined lattice constants are in agreement with those for undoped $MgWO_4$ (a = 4.6889 Å, b = 5.6753 Å, c = 4.9289 Å, $\beta = 90.726^o$) [21].

4.2 Doping concentration

The Ho^{3+} ion concentration N_{Ho} in the as-grown crystal was determined by inductively coupled plasma atomic emission spectrometry (ICP-AES). The measured N_{Ho} value was 1.207×10^{20} cm^{-3} (equivalently, 0.86 at.%). The effective segregation coefficient of Ho^{3+} ions $K_{Ho} = N_{measured}/N_{solution}$ was thus determined to be 0.086.

In $MgWO_4$, the Ho^{3+} ions are expected to replace the Mg^{2+} ones in a single type of sites (C_2 symmetry, VI-fold O^{2-} coordination). The charge compensation is provided by Na^+ cations present in the solution. The corresponding ionic radii are as following: Ho^{3+} (0.901 Å), Mg^{2+} (0.72 Å) and Na^+ (1.02 Å). Their comparison leads to the following conclusions. The larger ionic radius of Ho^{3+} and Na^+ compared to that of Mg^{2+} explains the larger lattice constants of Ho^{3+}:$MgWO_4$ relative to undoped $MgWO_4$ and the low segregation coefficient K_{Ho}. In addition, the substantial difference between the ionic radii of Ho^{3+} and Mg^{2+}, as well as the presence of Na^+ cations in the lattice promote a strong crystal-field for the active ions.

4.3 Thermal expansion

The thermal expansion of Ho^{3+}:$MgWO_4$ was studied using high-temperature XRD. The XRD patterns were recorded at temperature T ranging from 300 K to 800 K with a step of 50 K. The (a, b, c and β) values were determined for each T. All studied lattice constants increased linearly with T, see Fig. 2. The volume of the unit-cell V and crystal density ρ_{calc} were then calculated. The unit-cell of Ho^{3+}:$MgWO_4$ expanded with temperature and the density decreased almost linearly.

From Fig. 2(a-c), we calculated the coefficients of the linear thermal expansion α_T along the ***a***, ***b*** and ***c*** crystallographic axes as $\alpha_i = \Delta L_i/(L_i\Delta T)$ (i = a, b, c). The obtained values are α_a = 11.22, α_b = 8.09 and α_c = 8.77 [10^{-6} K^{-1}]. Previously, the α_T coefficients were measured for Cr^{3+}:$MgWO_4$ by a dilatometric method (at 283-923 K) as α_a = 10.5, α_b = 15.7 and α_c = 10.8 [10^{-6} K^{-1}] [13], hence the α_b value of Ho^{3+}:$MgWO_4$ is considerably smaller.

For a monoclinic crystal, the linear thermal expansion is described by a tensor α_{ij} which has a diagonal form α'_{mn} = diag(α'_{11}, α'_{22}, α'_{33}) in the eigen-frame of the three orthogonal principal axes X'_k (k = 1, 2, 3) [22]. Only one of these axes (X'_2) coincides with the two-fold (C_2) symmetry axis (***b***-axis, in our case). The remaining two axes (X'_1 and X'_3) are located in the mirror plane (the ***a***-***c*** plane). The α_{ij} tensor in the crystallographic frame {***a***, ***b***, ***c****}, where ***c**** =***a*** × ***b***, can be written as:

$$\alpha_{ij} = \begin{bmatrix} \alpha_a & 0 & \alpha_{ac^*} \\ 0 & \alpha_b & 0 \\ \alpha_{ac^*} & 0 & \alpha_{c^*} \end{bmatrix}, \quad (1)$$

where, α_{c^*} = 8.65 [10^{-6} K^{-1}] is the thermal expansion along the ***c****-axis, determined as $\Delta c^*/(c^*\Delta T)$, where $c^* = c\cdot\cos(\beta - 90°)$ [23], and α_{ac^*} are the non-diagonal elements. They can be calculated from the measured thermal expansion coefficients using the formula $\alpha_{\boldsymbol{m}} = m_i m_j \alpha_{ij}$, where ***m*** is the vector of direction cosines [22]. The diagonalization of the thermal expansion tensor by solving the equation $\det(\alpha_{ij} - \lambda\delta_{ij}) = 0$ leads to the following eigen-values: α'_{11} = 14.80, $\alpha'_{22} = \alpha_b$ = 8.09 and α'_{33} = 5.07 [10^{-6} K^{-1}] which determine the volumetric thermal expansion $\alpha_{vol} = \alpha'_{11} + \alpha'_{22} + \alpha'_{33}$ = 27.96 [10^{-6} K^{-1}]. The orientation of the X'_k axes is given in Fig. 3. The

X'_1 axis is counter-clockwise rotated at an angle θ of 37.35° from the ***a***-axis in the ***a-c*** plane (if the ***b***-axis is pointing towards the observer).

The anisotropy of the thermal expansion for Ho^{3+}:$MgWO_4$ is moderate, α'_{11}:α'_{33} = 2.9 and α'_{22}:α'_{33} = 1.6. This rather low anisotropy is favorable for power scaling of Ho^{3+}:$MgWO_4$ lasers, because it will reduce the probability of thermally induced cracking. It is also favorable for the crystal growth. For monoclinic Ho^{3+}:$KY(WO_4)_2$, this anisotropy is much stronger, α'_{33} : α'_{22} = 6.6 and α'_{11} : α'_{22} = 3.1 [23]. The anisotropy of the thermal expansion, the relatively high α_T values along certain directions, as well as the negative thermo-optic coefficients (dn/dT) of $MgWO_4$ [15] should determine the existence of athermal directions allowing for microchip laser operation.

5. Optical spectroscopy

5.1 Refractive index

$MgWO_4$ is an optically biaxial crystal. Its optical properties are thus described in the frame of three mutually orthogonal optical indicatrix axes {N_p, N_m, N_g} with the corresponding principal refractive indices $n_p < n_m < n_g$. One of the optical indicatrix axes (N_m) coincides with the "special" axis of this monoclinic crystal (the C_2 symmetry axis) and the remaining two (N_p and N_g) are located in the orthogonal plane [24]. For $MgWO_4$, the C_2-axis is parallel to the crystallographic ***b***-axis and the orthogonal plane is then ***a-c***. The angles $\varphi = \boldsymbol{a}\wedge N_g = 36.4°$ and $\psi = \boldsymbol{c}\wedge N_p = 37.1°$.

The information about the refractive index of $MgWO_4$ is scarce. Recently, we have quantified the refractive index anisotropy of $MgWO_4$ at ~1.2 μm as n_p = 1.97, n_m = 2.03 and n_g = 2.13±0.02 (the mean value: $\langle n\rangle_{exp}$ = 2.04) using transmission measurements [15]. Independently, Bhuyan *et al.* analyzed the dispersion of the refractive index of $MgWO_4$ theoretically using the density functional theory within the random phase approximation [25]. The results of this theoretical work ($\langle n\rangle_{calc}$ = 2.04) agrees well with our estimation. Thus, we fitted the data from [25] using a two-pole Sellmeier equation:

$$\langle n\rangle^2 = A + \frac{B\lambda^2}{\lambda^2 - C} + \frac{D\lambda^2}{\lambda^2 - E}, \qquad (2)$$

where, *A*–*E* are the Sellmeier coefficients and λ is the light wavelength in μm. The best-fit *A*–*E* values are listed in Table 1. The dispersion of the mean refractive index of $MgWO_4$ is shown in Fig. 4. In particular, at ~2 μm, $\langle n\rangle_{calc}$ = 1.99.

5.2 Optical absorption

Due to the available crystal dimensions, we cut a rectangular sample oriented in the crystallographic frame {***a***, ***b***, ***c****}, where ***c**** ⊥ ***a***. For Ho^{3+}:$MgWO_4$, the monoclinic angle β (***a***^***c***) is close to 90 ° (β = 90.744°) so the three polarizations available with this sample can be indicated as ***E*** ∥ ***a***, ***b***, ***c*** for simplicity (in other words, ***c**** ≈ ***c***). The sample dimensions were 2.76(***a***) × 3.01(***b***) × 2.54(***c****) mm^3. All six faces were polished to laser quality.

The RT absorption spectra of Ho^{3+}:$MgWO_4$ are shown in Fig. 5 for light polarizations ***E*** ∥ ***a***, ***b***, ***c***. The spectra are strongly polarized in agreement with the low symmetry (C_2) of the Ho^{3+} site; the maximum absorption corresponds to ***E*** ∥ ***b***. In the spectra, the bands are due to the

transitions from the ground-state ($^5I_8$) to the excited-states (from $^5I_7$ to (^5G,^3H)$_5$+$^3H_6$). The assignment of the latter is according to Ref. [26]. The transitions to the $^5I_5$ and $^5I_4$ excited-states, expected at ~0.90 and 0.75 μm, respectively, are too weak and cannot be clearly resolved.

In the visible, a broad and weak absorption at 0.4-0.6 μm underlying the Ho^{3+} bands is due to the color centers related to cationic vacancies. A combination of the color center absorption and the Ho^{3+} absorption determines the weak yellow-brown crystal coloration. The UV absorption edge is at ~340 nm (experimental bandgap: E_g = 3.6 eV). In [25], an indirect bandgap of 3.39 eV was determined from the first principles band calculation based on density functional theory and the experimental value for an undoped polycrystalline material was 4.17 eV.

5.3 Judd-Ofelt analysis

The transition intensities of Ho^{3+} ions in $MgWO_4$ were analyzed within the standard Judd-Ofelt (J-O) theory [27,28] and its modification (mJ-O) [29,30]. For the standard J-O theory, the electric dipole (ED) line strengths of the J → J' transitions are calculated as:

$$\langle S^{\mathrm{ED}}_{\mathrm{calc}}\rangle(JJ') = \sum_{k=2,4,6} U^{(k)}\Omega_k. \tag{3a}$$

$$U^{(k)} = \langle (4f^n)SLJ \,\|U^k\|\, (4f^n)S'L'J'\rangle^2. \tag{3b}$$

Here, $U^{(k)}$, are the reduced squared matrix elements and Ω_k are the intensity (J–O) parameters (for both, k = 2, 4, 6). The mJ-O theory includes the effect of configuration interaction. If only the excited configuration with opposite parity $4f^{n-1}5d^1$ contributes to configuration interaction, the intensity parameters are the linear functions of the energies of the two multiplets (E_J and $E_{J'}$) according to [29]:

$$\tilde{\Omega}_k = \Omega_k[1 + 2\alpha(E_J + E_{J'} - 2E_f^0)]. \tag{4}$$

Here, E_f^0 is the mean energy of the $4f^n$ configuration and $\alpha \approx 1/(2\Delta)$, where Δ has the meaning of the energy of the excited configuration $4f^{n-1}5d^1$.

This formalism was applied to the ED contributions of the f-f transition intensities of Ho^{3+} ions. The contribution of magnetic-dipole (MD) transitions with $\Delta J = J - J' = 0, \pm 1$ [31] was calculated separately within the Russell–Saunders approximation on wave functions of Ho^{3+} ion under the assumption of a free-ion.

First, we determined the experimental oscillator strengths $\langle f^{\Sigma}_{\mathrm{exp}}\rangle$ for transitions in absorption, $^5I_8 \rightarrow {}^{2S+1}L_J$. Here, the brackets indicate averaging over the three studied light polarizations, i.e., $\langle f\rangle = 1/3(f(\boldsymbol{a}) + f(\boldsymbol{b}) + f(\boldsymbol{c}))$. The set of $\langle f^{\Sigma}_{\mathrm{exp}}\rangle$ was analyzed within both the J-O and mJ-O theories to determine the intensity parameters, $\{\Omega_k\}$ and $\{\Omega_k, \alpha\}$, respectively, where k = 2, 4, 6. Both the experimental $\langle f^{\Sigma}_{\mathrm{exp}}\rangle$ and the calculated $\langle f^{\Sigma}_{\mathrm{calc}}\rangle$ absorption oscillator strengths are listed in Table 2. Here, the superscript Σ indicates that the f values include both the ED and MD contributions. The refractive index for each barycenter of the absorption band $\langle\lambda\rangle$ was calculated from the dispersion curve, Eq. (2). Accounting for the dispersion of the refractive index of the host matrix is important for adequate application of the J-O theory [32]. The reduced squared matrix elements $U^{(k)}$, k = 2, 4, 6 are according to Ref. [1].

The determined intensity parameters for both J-O and mJ-O theories are listed in Table 3. In the former case, Ω_2 = 17.57, Ω_4 = 3.90 and Ω_6 = 1.69 [10^{-20} cm^2]. These values are close to those

for monoclinic Ho^{3+}:$KGd(WO_4)_2$ crystal, $\Omega_2 = 15.35$, $\Omega_4 = 3.79$ and $\Omega_6 = 1.69$ [10^{-20} cm^2] [33]. The root mean square (rms) deviation between the $\langle f^{\Sigma}_{exp} \rangle$ and $\langle f^{\Sigma}_{calc} \rangle$ values is much lower for the modified J-O theory (0.187) as compared to the standard one (0.534). Because of this, we selected the mJ-O theory for further description of radiative spontaneous transitions.

Using the determined intensity parameters $\{\Omega_k, \alpha\}$ within the mJ-O theory, we calculated the probabilities of radiative spontaneous transition $A^{\Sigma}_{calc}(JJ')$ (here, the superscript Σ indicates the sum of both the ED and MD contributions), the luminescence branching ratios $B(JJ')$ and the radiative lifetimes of the excited states τ_{rad}, Table 4. The refractive index for each mean emission wavelength $\langle \lambda \rangle$ was calculated from the dispersion curve, Eq. (2). The radiative lifetime of the upper laser level ($^5I_7$) is 6.18 ms.

5.4 Luminescence

Polarized luminescence spectra of the Ho^{3+}:$MgWO_4$ crystal are shown in Fig. 6. In the near-IR, Fig. 6(a), a broad emission band spanning from 1.85 to 2.12 μm was observed and assigned to the $^5I_7 \rightarrow {}^5I_8$ transition.

In the visible, Fig. 6(b), several emissions in the green (at 0.54-0.56 μm, $^5S_2+{}^5F_4 \rightarrow {}^5I_8$ transition) and red spectral ranges (at 0.64-0.67 μm, $^5F_5 \rightarrow {}^5I_8$ transition and at 0.74-0.77 μm, $^5S_2+{}^5F_4 \rightarrow {}^5I_7$ transition) were observed.

5.5 Stark splitting

By using low-temperature (6 K) absorption and the luminescence studies for the $^5I_8 \leftrightarrow {}^5I_7$ transition (Fig. 7), we determined the Stark splitting of the ground-state ($^5I_8$) and the upper laser level ($^5I_7$) of the Ho^{3+} ion, Fig. 8.

For the C_2 symmetry site and integer J, each $^{2S+1}L_J$ multiplet has $2J+1$ Stark components. All of them were resolved. The total Stark splitting of the ground-state $\Delta(^5I_8)$ is 380 cm^{-1}. This splitting is much larger than in monoclinic Ho^{3+}:$KY(WO_4)_2$ for which $\Delta(^5I_8)$ is 281 cm^{-1} [23]. The zero-phonon-line (ZPL), i.e., the transition between the lowest Stark sub-levels of both multiplets, is observed at E_{ZPL} = 5143 cm^{-1} (1944 nm). It is blue-shifted with respect to Ho^{3+}:$KY(WO_4)_2$ (E_{ZPL} = 5100 cm^{-1}) [23]. The longest wavelength of the purely electronic transition is 2100 nm (larger than in Ho^{3+}:$KY(WO_4)_2$: 2075 nm).

The increased Stark splitting for Ho^{3+} in monoclinic $MgWO_4$ as compared to $KY(WO_4)_2$ indicates a stronger crystal-field of the former material, promoted by the substantial difference between the ionic radii of Ho^{3+}, Na^+ and Mg^{2+}. Note that the Ho^{3+} site symmetry for both crystals is the same (C_2).

5.6 Transition cross-sections

The absorption cross-sections were determined from the measured absorption spectra, $\sigma_{abs} = \alpha_{abs}/N_{Ho}$, Fig. 9(a). For the $^5I_8 \rightarrow {}^5I_7$ transition used for in-band pumping of Ho^{3+} ions, the maximum σ_{abs} is 0.96×10^{-20} cm^2 at 1944.5 nm for light polarization $\boldsymbol{E} \parallel \boldsymbol{b}$. The full width at half maximum (FWHM) of this peak is 18.2 nm. For $\boldsymbol{E} \parallel \boldsymbol{a}$ and $\boldsymbol{E} \parallel \boldsymbol{c}$, the peak σ_{abs} is about 1.3 times lower while the FWHM is similar, ~19 nm. For the same transition of Ho^{3+} in monoclinic

$KY(WO_4)_2$, the maximum σ_{abs} is higher, 1.60×10^{-20} cm^2 at 1961.0 nm while the corresponding FWHM is smaller, only 12.1 nm (for $\boldsymbol{E} \parallel N_m$) [23].

The stimulated-emission (SE) cross-sections of Ho^{3+}:$MgWO_4$, σ_{SE}, were determined with the reciprocity method (RM) [34]:

$$\sigma_{SE}^{i}(\lambda) = \sigma_{abs}^{i}(\lambda)\frac{Z_1}{Z_2}\exp(-\frac{hc/\lambda - E_{ZPL}}{kT}), \tag{5a}$$

$$Z_m = \sum_k g_k^m \exp(-E_k^m / kT). \tag{5b}$$

Here, σ_{abs} is the absorption cross-section, i indicates the polarization state, h is the Planck constant, c is the speed of light, k is the Boltzmann constant, T is the crystal temperature (RT), E_{ZPL} is the energy difference between the lowest Stark sub-levels of the two multiplets (zero phonon line (ZPL), 5143 cm^{-1}, Fig. 8), and Z_m are the partition functions of the lower (m = 1) and the upper (m =2) manifolds. $g^m{}_k$ (assumed to be 1) is the degeneracy of the sub-level with the number k and energy $E^m{}_k$ measured from the lowest sub-level of the multiplet. Using Eq. 5(b) and the determined Stark splitting, Fig. 8, we calculated the partition functions Z_1 = 9.80 and Z_2 = 8.87, so that Z_1/Z_2 = 1.11.

The results on σ_{SE} are shown in Fig. 9(b). The maximum σ_{SE} is 1.82×10^{-20} cm^2 at 2083.3 nm for $\boldsymbol{E} \parallel \boldsymbol{b}$. For the other two polarizations, the SE cross-sections are lower, namely 1.66×10^{-20} cm^2 at 2068.4 nm (for $\boldsymbol{E} \parallel \boldsymbol{a}$) and 0.60×10^{-20} cm^2 at 2069.5 nm (for $\boldsymbol{E} \parallel \boldsymbol{c}$). Such a strong anisotropy will promote the natural selection of a linearly polarized radiation in Ho^{3+}:$MgWO_4$ lasers. For Ho^{3+}:$KY(WO_4)_2$, the maximum σ_{SE} is higher, 2.65×10^{-20} cm^2 at 2056.3 nm for $\boldsymbol{E} \parallel N_m$ [23].

Thus, the study of the absorption and SE cross-section spectra of Ho^{3+}:$MgWO_4$ indicates a broadening of the spectral bands with respect to Ho^{3+}:$KY(WO_4)_2$ while the peak cross-sections are still rather high for certain light polarizations.

The Ho^{3+} ions represent a quasi-three-level laser scheme and the gain cross-sections, $\sigma_{gain} = \beta\sigma_{SE} - (1-\beta)\sigma_{abs}$, are determined to predict the possible laser wavelengths. Here, $\beta = N_2(^5I_7)/N_{Ho}$ is the inversion ratio. The results for light polarizations $\boldsymbol{E} \parallel \boldsymbol{a}$ and $\boldsymbol{E} \parallel \boldsymbol{b}$ are shown in Fig. 10. For small $\beta < 0.15$ the gain spectrum of $\boldsymbol{E} \parallel \boldsymbol{b}$ is smooth and it spans from 2.10 to 2.14 μm. For higher inversion, a broad local peak centered at ~2085 nm dominates in the spectra. The gain bandwidth (FWHM) $\Delta\lambda_g$ is ~27 nm for β = 0.20. For $\boldsymbol{E} \parallel \boldsymbol{a}$, with the increase of the inversion ratio, several local peaks at ~2110, 2096 and 2070 nm are observed.

The gain bandwidth is as broad as ~55 nm. For Ho^{3+}:$KY(WO_4)_2$, $\Delta\lambda_g$ is about 26 nm for $\boldsymbol{E} \parallel N_m$ [23]. The broad emission bands of Ho^{3+} in $MgWO_4$ are promising for mode-locked lasers.

5.7 Luminescence decay

The luminescence decay curve of Ho^{3+}:$MgWO_4$ is shown in Fig. 11. The decay is single-exponential, which agrees with a single type of sites for Ho^{3+} ions in $MgWO_4$. The corresponding luminescence decay time τ_{lum} is 4.40 ms. It is slightly shorter than that for 3 at.% Ho^{3+}:$KY(WO_4)_2$ (4.8 ms). The luminescence quantum yield:

$$\eta_q = \frac{\tau_{lum}}{\tau_{rad}}. \tag{6}$$

For Ho^{3+}:$MgWO_4$, η_q = 71%. Note that the maximum phonon frequency of $MgWO_4$ is relatively high, $h\nu_{ph}$ = 916 cm^{-1} [7], compared to the energy gap between the $^5I_7$ and $^5I_8$ states (4763 cm^{-1}).

5.8 Towards Tm^{3+},Ho^{3+} codoping

Tm^{3+}, Ho^{3+} codoping is a well-known scheme of sensitization of Ho^{3+} ions leading to low-threshold laser operation [35]. Tm^{3+} ions have a strong absorption at around ~0.8 μm ($^3H_6 \rightarrow {}^3H_4$ transition) and they provide an energy transfer (ET) of electronic excitation to the Ho^{3+} ions, $^3F_4(Tm^{3+}) \rightarrow {}^5I_7(Ho^{3+})$ [36]. Efficient Tm^{3+}, Ho^{3+} codoped MDT lasers were realized [37]. The ET process in Tm^{3+}:$MgWO_4$ is promoted by the fact that the barycenter of the $^3F_4$ state (5844 cm^{-1} for [15]) is higher than that of the $^5I_7$ state (5269 cm^{-1}).

For Tm^{3+}, Ho^{3}+ codoped materials, the ratio of parameters of the $Ho^{3+} \rightarrow Tm^{3+}$ back ET to the $Tm^{3+} \rightarrow Ho^{3+}$ ET is called the equilibrium constant Θ. It is concentration-independent and it can be deduced from the Stark splitting of the Tm^{3+} and Ho^{3+} ions, namely [38]:

$$\Theta = \frac{Z(^3F_4)\cdot Z(^5I_8)}{Z(^3H_6)\cdot Z(^5I_7)} \exp\left(-\frac{(E_{ZPL}^{Tm} - E_{ZPL}^{Ho})}{kT}\right), \quad (7)$$

where k is the Boltzmann constant, T is the crystal temperature. For Tm^{3+},Ho^{3+}:$MgWO_4$, Θ = 0.110 which is close to the value for Tm^{3+},Ho^{3+}:$KY(WO_4)_2$ (Θ = 0.07) [39] and for such well-known hosts for Tm^{3+},Ho^{3+} codoping as $Y_3Al_5O_{12}$ (Θ = 0.12) and $LiYF_4$ (Θ = 0.12) [38].

Besides the low-threshold lasing expected for Tm^{3+},Ho^{3+}:$MgWO_4$, this material is interesting for its spectrally broad gain bandwidth at >2 μm, e.g., for applications in mode-locked and in particular femtosecond lasers [40,41].

6. Laser operation

6.1 Laser set-up

The laser experiments were performed with the same Ho^{3+}:$MgWO_4$ sample which was used in the spectroscopic studies. It was oriented for light propagation along the ***a***-axis (thickness t = 2.76 mm). The 3.01(***b***) × 2.54(***c****) mm^2 aperture faces were polished to laser quality and remained uncoated. The laser crystal was mounted on an Al holder with a thermal contact from one lateral side. The Al holder was passively-cooled. A plano-plano (microchip-type) laser cavity was used. It consisted of a flat dichroic pump mirror (PM) coated for high transmission (HT, T > 86%) at 1.9–2.0 μm and for high reflection (HR, R > 98.5%) at 2.02–2.5 μm and a flat output coupler (OC) with the actual transmission at the laser wavelength T_{OC} of 0.5% or 2.4%. The transmission spectra of the cavity mirrors were measured using the spectrophotometer. Both cavity mirrors were placed as close as possible to the laser crystal minimizing the air gaps. The total geometrical cavity length was thus close to the crystal thickness.

As a pump source, we used a diode-pumped Tm:$KLu(WO_4)_2$ microchip laser emitting up to 1.8 W of CW output at 1946 nm (TEM_{00} mode, M^2 < 1.1, linear polarization). More details about the design of the Tm laser can be found elsewhere [18]. Its output was collimated and focused into the Ho^{3+}:$MgWO_4$ crystal by a pair of plano-concave lenses with the focal lengths of 150 and 60 mm, respectively. The polarization of the pump corresponded to $\boldsymbol{E} \parallel \boldsymbol{b}$ in the crystal. The radius of the pump beam in the focus w_p was 100±10 μm. Due to the back reflection of the OC

at the pump wavelength (R > 98%), the crystal was pumped in a double-pass. The single-pass pump absorption was measured at the threshold pump power under non-lasing conditions to be $\eta_{1\text{-pass}}$ = 9±1%. From this value, the double-pass absorption was calculated accounting for the Fresnel losses at the uncoated crystal surfaces, $\eta_{2\text{-pass}}$ = 15±2%. The small-signal absorption at the pump wavelength, $\eta_{1\text{-pass},0} = 1 - \exp(-\sigma^{P}_{abs} N_{Ho} t) = 26\%$ which is higher than the experimental value due to the bleaching of the ground-state.

6.2 Laser performance

The input-output dependences and typical emission spectra of the Ho^{3+}:$MgWO_4$ laser are shown in Fig. 12. For T_{OC} = 0.5%, the output power reached 52 mW at ~2104 nm with a slope efficiency η of 72% (with respect to the absorbed pump power P_{abs}), see Fig. 12(a). The laser threshold was at P_{abs} = 0.16 W. For higher output coupling of 2.4%, the laser operated at shorter wavelength (~2091 nm) and the slope efficiency decreased to 49%. The deterioration of the laser performance for higher output coupling was also observed in in-band-pumped Ho^{3+}:MDT lasers and assigned to increased upconversion losses related to higher inversion [18,19]. The power scaling was limited by the low available pump power and the low absorption of the Ho^{3+}:$MgWO_4$ crystal. The output dependences were linear and no crystal fracture was observed.

The output polarization of the Ho^{3+}:$MgWO_4$ laser was linear ($\boldsymbol{E} \parallel \boldsymbol{b}$), i.e., parallel to one of the optical indicatrix axes (N_m); it was naturally selected by the anisotropy of the gain. The laser emission spectra, Fig. 12(b), are in agreement with the gain spectra, Fig. 10(b). The multi-peak spectral behavior was due to the etalon effects at the crystal-mirror interfaces.

7. Conclusion

$MgWO_4$ is a promising host material for Ho^{3+} doping. Due to the difference in ionic radii of the substituted (Mg^{2+}) and dopant (Ho^{3+}) ions, a significant broadening of the spectral bands is observed. The low site symmetry determines the strong polarization-anisotropy of the transition cross-sections. As a result, Ho^{3+}:$MgWO_4$ features a large Stark splitting of the ground-state (for an anisotropic crystal), $\Delta(^5I_8)$ = 380 cm^{-1}, relatively high stimulated-emission cross-section of 1.82×10^{-20} cm^2 at 2083.3 nm for a particular light polarization, $\boldsymbol{E} \parallel N_m$ ($\boldsymbol{b}$), high luminescence quantum yield (>70%) and a broad gain bandwidth reaching ~55 nm for $\boldsymbol{E} \parallel \boldsymbol{a}$. All these features together with the high thermal conductivity of $MgWO_4$ make Ho^{3+}:$MgWO_4$ attractive for efficient CW and ML bulk and thin-disk lasers at ~2.1 μm.

In the present work, we demonstrated the first laser operation of Ho^{3+}:$MgWO_4$ using in-band pumping at 1946 nm by a Tm-laser. A slope efficiency up to 72% was achieved and the laser operated at 2104 nm. Further power scaling is possible with (i) an increase of the Ho^{3+} concentration and (ii) the use of powerful pump sources, e.g., Tm fiber lasers or GaSb diodes. Further optimization of the growth and annealing conditions will allow one to improve the optical quality of Ho^{3+}:$MgWO_4$ crystals (i.e., reduce the effect of color centers). The growth of Tm^{3+},Ho^{3+} codoped MgWO4 crystals is also promising.

Acknowledgments

The present work has received funding through the following projects: Spanish Government (MAT2016-75716-C2-1-R (AEI/FEDER,UE) and TEC 2014-55948-R, and by Generalitat de Catalunya (2017SGR755). F.D. acknowledges additional support through the ICREA academia award 2010ICREA-02 for excellence in research. P.L. acknowledges financial support from the Government of the Russian Federation (Grant 074-U01) through ITMO Post-Doctoral Fellowship scheme. P.L. and K.S. acknowledge support by Russian Fund for Basic Research, grant No. 18-02-01058.

References

1. B. M. Walsh, N. P. Barnes, B. Di Bartolo, Branching ratios, cross sections, and radiative lifetimes of rare earth ions in solids: Application to Tm^{3+} and Ho^{3+} ions in $LiYF_4$, J. Appl. Phys. 83 (1998) 2772-2787.
2. B. M. Walsh, G. W. Grew, N. P. Barnes, Energy levels and intensity parameters of Ho^{3+} ions in $GdLiF_4$, $YLiF_4$ and $LuLiF_4$, J. Phys.: Cond. Matter 17 (2005) 7643-7665.
3. B. M. Walsh, G. W. Grew, N. P. Barnes, Energy levels and intensity parameters of Ho^{3+} ions in $Y_3Al_5O_{12}$ and $Lu_3Al_5O_{12}$, J. Phys. Chem. Solids 67 (2006) 1567-1582.
4. T. M. Taczak, D. K. Killinger, Development of a tunable, narrow-linewidth, cw 2.066-μm Ho:YLF laser for remote sensing of atmospheric CO_2 and H_2O, Appl. Opt. 37 (1998) 8460-8476.
5. U. N. Singh, B. M. Walsh, J. Yu, M. Petros, M. J. Kavaya, T. F. Refaat, N. P. Barnes, Twenty years of Tm:Ho:YLF and LuLiF laser development for global wind and carbon dioxide active remote sensing, Opt. Mater. Express 5 (2015) 827-837.
6. P. A. Budni, L. A. Pomeranz, M. L. Lemons, C. A. Miller, J. R. Mosto, E. P. Chicklis, Efficient mid-infrared laser using 1.9-μm-pumped Ho:YAG and $ZnGeP_2$ optical parametric oscillators, J. Opt. Soc. Am. B 17 (2000) 723-728.
7. L. Zhang, H. Lin, G. Zhang, X. Mateos, J. M. Serres, M. Aguiló, F. Díaz, U. Griebner, V. Petrov, Y. Wang, P. Loiko, E. Vilejshikova, K. Yumashev, Z. Lin, W. Chen, Crystal growth, optical spectroscopy and laser action of Tm^{3+}-doped monoclinic magnesium tungstate, Opt. Express 25 (2017) 3682-3693.
8. P. Loiko, J. M. Serres, X. Mateos, M. Aguiló, F. Díaz, L. Zhang, Z. Lin, H. Lin, G. Zhang, K. Yumashev, V. Petrov, U. Griebner, Y. Wang, S. Y. Choi, F. Rotermund, and W. Chen, Monoclinic Tm^{3+}:$MgWO_4$: a promising crystal for continuous-wave and passively Q-switched lasers at ~2 μm, Opt. Lett. 42 (2017) 1177-1180.
9. Y. Wang, W. Chen, M. Mero, L. Zhang, H. Lin, Z. Lin, G. Zhang, F. Rotermund, Y. J. Cho, P. Loiko, X. Mateos, U. Griebner, V. Petrov, Sub-100 fs Tm:$MgWO_4$ laser at 2017 nm mode-locked by a graphene saturable absorber, Opt. Lett. 42 (2017) 3076-3079.
10. E. Cavalli, A. Belletti, M. G. Brik, Optical spectra and energy levels of the Cr^{3+} ions in MWO_4 (M = Mg, Zn, Cd) and $MgMoO_4$ crystals, J. Phys. Chem. Solids 69 (2008) 29-34.
11. X. Wang, Z. Fan, H. Yu, H. Zhang, J. Wang, Characterization of $ZnWO_4$ Raman crystal, Opt. Mater. Express 7 (2017) 1732-1744.

12. P. Becker, L. Bohatý, H. J. Eichler, H. Rhee, A. A. Kaminskii, High-gain Raman induced multiple Stokes and anti-Stokes generation in monoclinic multiferroic $MnWO_4$ single crystals, Laser Phys. Lett. 4 (2007) 884-889.
13. L. Zhang, Y. Huang, S. Sun, F. Yuan, Z. Lin, G. Wang, Thermal and spectral characterization of Cr^{3+}:$MgWO_4$ – a promising tunable laser material, J. Lumin. 169, Part A (2016) 161-164.
14. Ò. Silvestre, J. Grau, M. C. Pujol, J. Massons, M. Aguiló, F. Díaz, M. T. Borowiec, A. Szewczyk, M. U. Gutowska, M. Massot, A. Salazar, V. Petrov, Thermal properties of monoclinic $KLu(WO_4)_2$ as a promising solid state laser host, Opt. Express 16 (2008) 5022-5034.
15. P. Loiko, L. Zhang, J.M. Serres, Y. Wang, M. Aguiló, F. Díaz, Z. Lin, H. Lin, G. Zhang, E. Vilejshikova, E. Dunina, A. Kornienko, L. Fomicheva, V. Petrov, U. Griebner, W. Chen, X. Mateos, Monoclinic Tm:$MgWO_4$ crystal: Crystal-field analysis, tunable and vibronic laser demonstration, J. Alloy Compd. 763 (2018) 581-591.
16. D. Y. Shen, A. Abdolvand, L. J. Cooper, W. A. Clarkson, Efficient Ho:YAG laser pumped by a cladding-pumped tunable Tm:silica-fibre laser, Appl. Phys. B 79 (2004) 559-561.
17. P. A. Budni, M. L. Lemons, J. R. Mosto, E. P. Chicklis, High-power/high-brightness diode-pumped 1.9-μm thulium and resonantly pumped 2.1-μm holmium lasers, IEEE J. Select. Top. Quantum Electron. 6 (2000) 629-635.
18. P. Loiko, J. M. Serres, X. Mateos, K. Yumashev, N. Kuleshov, V. Petrov, U. Griebner, M. Aguiló, F. Díaz, In-band-pumped Ho:$KLu(WO_4)_2$ microchip laser with 84% slope efficiency, Opt. Lett. 40 (2015) 344-347.
19. V. Jambunathan, X. Mateos, M. C. Pujol, J. J. Carvajal, F. Díaz, M. Aguiló, U. Griebner, V. Petrov, Continuous-wave laser generation at ~2.1 μm in Ho:$KRE(WO_4)_2$ (RE = Y, Gd, Lu) crystals: a comparative study, Opt. Express 19 (2011) 25279-25289.
20. X. Mateos, S. Lamrini, K. Scholle, P. Fuhrberg, S. Vatnik, P. Loiko, I. Vedin, M. Aguiló, F. Díaz, U. Griebner, V. Petrov, Holmium thin-disk laser at ~2056 nm based on Ho:$KY(WO_4)_2$ / $KY(WO_4)_2$ epitaxy with 60% slope efficiency and simplified pump geometry, Opt. Lett. 42 (2017) 3490-3493.
21. V. B. Mikhailik, H. Kraus, V. Kapustyanyk, M. Panasyuk, Y. Prots, V. Tsybulskyi, L. Vasylechko, Structure, luminescence and scintillation properties of the $MgWO_4$–$MgMoO_4$ system, J. Phys. Condens. Matter 20 (2008) 365219.
22. P. A. Loiko, K. V. Yumashev, N. V. Kuleshov, G. E. Rachkovskaya, A. A. Pavlyuk, Detailed characterization of thermal expansion tensor in monoclinic $KRe(WO_4)_2$ (where Re = Gd, Y, Lu, Yb), Opt. Mater. 34 (2011) 23-26.
23. V. Jambunathan, X. Mateos, P.A. Loiko, J.M. Serres, U. Griebner, V. Petrov, K.V. Yumashev, M. Aguiló, F. Díaz, Growth, spectroscopy and laser operation of Ho:$KY(WO_4)_2$, J. Lumin. 179 (2016) 50-58.
24. L. Zhang, W. Chen, J. Lu, H. Lin, L. Li, G. Wang, G. Zhang, Z. Lin, Characterization of growth, optical properties, and laser performance of monoclinic Yb:$MgWO_4$ crystal, Opt. Mater. Express 6 (2016) 1627-1634.

25. P.D. Bhuyan, D. Singh, S. Kansara, P. Yadav, S.K. Gupta, Y. Sonvane, S.K. Rout, and E. Sinha, Experimental and theoretical analysis of electronic and optical properties of $MgWO_4$, J. Mater. Sci. 52 (2017) 4934-4943.
26. W. T. Carnall, P. R. Fields, K. Rajnak, Electronic energy levels in the trivalent lanthanide aquo ions. I. Pr^{3+}, Nd^{3+}, Pm^{3+}, Sm^{3+}, Dy^{3+}, Ho^{3+}, Er^{3+}, and Tm^{3+}, J. Chem. Phys. 49 (1968) 4424-4442.
27. B. R. Judd, Optical absorption intensities of rare-earth ions, Phys. Rev. 127 (1962) 750–761.
28. G. S. Ofelt, Intensities of crystal spectra of rare-earth ions, J. Chem. Phys. 37 (1962) 511–520.
29. A.A. Kornienko, A.A. Kaminskii, E.B. Dunina, Dependence of the line strength of f–f transitions on the manifold energy. II. Analysis of Pr^{3+} in $KPrP_4O_{12}$, Phys. Status Solidi (b) 157 (1990) 267-273.
30. P. Loiko, A. Volokitina, X. Mateos, E. Dunina, A. Kornienko, E. Vilejshikova, M. Aguilo, F. Diaz, Spectroscopy of Tb^{3+} ions in monoclinic $KLu(WO_4)_2$ crystal: application of an intermediate configuration interaction theory, Opt. Mater. 78 (2018) 495-501.
31. C. M. Dodson, R. Zia, Magnetic dipole and electric quadrupole transitions in the trivalent lanthanide series: Calculated emission rates and oscillator strengths, Phys. Rev. B 86 (2012) 125102.
32. M.P. Hehlen, M.G. Brik, K.W. Krämer, 50^{th} anniversary of the Judd–Ofelt theory: An experimentalist's view of the formalism and its application, J. Lumin. 136 (2013) 221-239.
33. M.C. Pujol, J. Massons, M. Aguiló, F. Díaz, M. Rico, and C. Zaldo, Emission cross sections and spectroscopy of Ho^{3+} laser channels in $KGd(WO_4)_2$ single crystal, IEEE J. Quantum Electron. 38 (2002) 93-100.
34. S. A. Payne, L. L. Chase, L. K. Smith, W. L. Kway, W. F. Krupke, Infrared cross-section measurements for crystals doped with Er^{3+}, Tm^{3+} and Ho^{3+}, IEEE J. Quantum Electron. 28 (1992) 2619-2630.
35. T. Y. Fan, G. Huber, R. L. Byer, P. Mitzscherlich, Spectroscopy and diode laser-pumped operation of Tm, Ho: YAG, IEEE J. Quantum Electron. 24 (1988) 924-933.
36. B. M. Walsh, N. P. Barnes, B. Di Bartolo, On the distribution of energy between the Tm $^3F_4$ and Ho $^5I_7$ manifolds in Tm-sensitized Ho luminescence, J. Lumin. 75 (1997) 89-98.
37. P. Loiko, J.M. Serres, X. Mateos, K. Yumashev, N. Kuleshov, V. Petrov, U. Griebner, M. Aguiló, F. Díaz, Microchip laser operation of Tm,Ho:$KLu(WO_4)_2$ crystal, Opt. Express 22 (2014) 27976-27984.
38. B. M. Walsh, N. P. Barnes, B. Di Bartolo, The temperature dependence of energy transfer between the Tm $^3F_4$ and Ho $^5I_7$ manifolds of Tm-sensitized Ho luminescence in YAG and YLF, J. Lumin. 90 (2000) 39-48.
39. A. A. Lagatsky, F. Fusari, S. V. Kurilchik, V. E. Kisel, A. S. Yasukevich, N. V. Kuleshov, A. A. Pavlyuk, C. T. A. Brown, W. Sibbett, Optical spectroscopy and efficient continuous-wave operation near 2 μm for a Tm,Ho:KYW laser crystal, Appl. Phys. B 97 (2009) 321-326.

40. Y. Zhao, Y. Wang, X. Zhang, X. Mateos, Z. Pan, P. Loiko, W. Zhou, X. Xu, J. Xu, D. Shen, S. Suomalainen, A. Härkönen, M. Guina, U. Griebner, V. Petrov, 87-fs mode-locked Tm,Ho:$CaYAlO_4$ laser at ~2043 nm, Opt. Lett. 43 (2018) 915-918.
41. Y. Zhao, Y. Wang, W. Chen, Z. Pan, L. Wang, X. Dai, H. Yuan, Y. Zhang, H. Cai, J. E. Bae, S. Y. Choi, F. Rotermund, P. Loiko, J. M. Serres, X. Mateos, W. Zhou, D. Shen, U. Griebner, V. Petrov, 67-fs pulse generation from a mode-locked Tm,Ho:CLNGG laser at 2083 nm, Opt. Express 27 (2019) 1922-1928.

Table 1. Sellmeier coefficients* for the mean refractive index ⟨*n*⟩ of $MgWO_4$.

Coefficient	Value
A	1.520
B, μm^{-2}	2.503
C, μm^2	0.068
D, μm^{-2}	0.648
E, μm^2	32.0

*A-E – Sellmeier coefficients, according to Eq. (2).

Table 2. Measured and calculated absorption oscillator strengths of Ho^{3+} in $MgWO_4$.

Transition $^5I_8 \rightarrow {}^{2S+1}L_J$	‹λ›, nm	‹Γ›, cm^{-1}nm	$U^{(2)}$	$U^{(4)}$	$U^{(6)}$	‹f^{exp}› ×10^6	‹f^{calc}›×10^6	
							J-O	mJ-O
$^5I_7$	1944.0	86.5	0.0249	0.1344	1.5216	2.14	2.09^{ED}+ 0.56^{MD}	1.77^{ED}+ 0.56^{MD}
$^5I_6$	1168.3	16.7	0.0084	0.0386	0.6921	1.14	1.41^{ED}	1.27^{ED}
$^5F_5$	648.4	17.9	0	0.4250	0.5687	4.00	4.58^{ED}	4.22^{ED}
$^5F_4$+$^5S_2$	541.6	17.6	0	0.2392	0.9339	5.63	5.29^{ED}	5.32^{ED}
$^5F_3$	489.6	3.58	0	0	0.3464	1.41	1.36^{ED}	1.49^{ED}
$^5F_2$	474.0	1.90	0	0	0.2041	0.79	0.83^{ED}	0.94^{ED}
$^5G_6$+$^5F_1$	448.0	156.0	1.5409	0.8744	0.2946	72.74	73.02^{ED}	72.74^{ED}
$(^5G,^3G)_5$	420.7	10.0	0	0.5338	0.0002	5.31	5.47^{ED}	5.27^{ED}
$^3K_7$+$^5G_4$	386.2	1.87	0.0058	0.0361	0.0697	1.17	1.04^{ED}+ 0.005^{MD}	1.11^{ED}+ 0.005^{MD}
$^3H_6$+$(^5G,^3H)_5$	361.5	29.5	0.2155	0.1969	0.1679	21.12	19.95^{ED}	21.23^{ED}
r.m.s. dev.							*0.534*	*0.187*

‹λ› - "center of gravity" of the absorption band, ‹Γ› – integrated absorption coefficient, $U^{(k)}$ – squared reduced matrix elements, ‹f^{exp}› and ‹f^{calc}› – experimental and calculated absorption

oscillator strengths, respectively, ED and MD stand for the electric-dipole and magnetic-dipole contributions, respectively.

Table 3. Parameters of the "standard" and modified Judd-Ofelt theories applied for Ho^{3+} ions in monoclinic $MgWO_4$.

Parameter	Theory	
	J-O	mJ-O
$\Omega_2\times10^{20}$, cm^2	17.57	21.09
$\Omega_4\times10^{20}$, cm^2	3.90	4.42
$\Omega_6\times10^{20}$, cm^2	1.69	2.28
$\alpha\times10^4$, cm	–	0.053

Table 4. Calculated probabilities of the spontaneous radiative transitions of Ho^{3+} in $MgWO_4$.

Transition	$\langle\lambda\rangle$, nm	$U^{(2)}$	$U^{(4)}$	$U^{(6)}$	$A^{\Sigma}_{calc}(JJ')$, s^{-1}	$B(JJ')$, %	A_{tot}, s^{-1}	τ_{rad}, ms
$^5I_7\rightarrow{}^5I_8$	1944	0.0249	0.1344	1.5217	$122.8^{ED}+39.1^{MD}$	100	161.9	6.18
$^5I_6\rightarrow{}^5I_7$	2927	0.0319	0.1336	0.9308	$34.8^{ED}+19.0^{MD}$	16.0	336.1	2.98
$^5I_6\rightarrow{}^5I_8$	1168	0.0083	0.0383	0.6918	282.3^{ED}	84.0		
$^5I_5\rightarrow{}^5I_6$	3790	0.0438	0.1705	0.5729	$15.8^{ED}+8.8^{MD}$	9.2	268.6	3.72
$^5I_5\rightarrow{}^5I_7$	1652	0.0027	0.0226	0.8887	141.8^{ED}	52.8		
$^5I_5\rightarrow{}^5I_8$	893	0	0.0099	0.0936	102.2^{ED}	38.0		
$^5I_4\rightarrow{}^5I_5$	4911	0.0312	0.1237	0.9099	$12.1^{ED}+3.9^{MD}$	9.3	172.2	5.81
$^5I_4\rightarrow{}^5I_6$	2139	0.0022	0.0281	0.6640	66.6^{ED}	38.7		
$^5I_4\rightarrow{}^5I_7$	1236	0	0.0033	0.1568	74.5^{ED}	43.2		
$^5I_4\rightarrow{}^5I_8$	755.6	0	0	0.0077	15.1^{ED}	8.8		
$^5F_5\rightarrow{}^5I_4$	4521	0.0001	0.0059	0.0040	$0.2^{ED}+0.03^{MD}$	<0.1	4857	0.21
$^5F_5\rightarrow{}^5I_5$	2367	0.0068	0.0271	0.1649	$18.3^{ED}+0.8^{MD}$	0.4		
$^5F_5\rightarrow{}^5I_6$	1457	0.0102	0.1213	0.4995	$212.7^{ED}+2.6^{MD}$	4.4		
$^5F_5\rightarrow{}^5I_7$	972.9	0.0177	0.3298	0.4340	1024^{ED}	21.0		
$^5F_5\rightarrow{}^5I_8$	648.4	0	0.4277	0.5686	3598^{ED}	74.1		
$^5S_2+{}^5F_4\rightarrow{}^5F_5$	3588	0	0.0256	0.2783	$66.1^{ED}+6.3^{MD}$	0.6	13131	0.08
$^5S_2+{}^5F_4\rightarrow{}^5I_4$	2009	0	0.0212	0.3693	$139.2^{ED}+0.1^{MD}$	1.0		
$^5S_2+{}^5F_4\rightarrow{}^5I_5$	1425	0.0001	0.0459	0.1558	$388.6^{ED}+0.2^{MD}$	3.0		
$^5S_2+{}^5F_4\rightarrow{}^5I_6$	1036	0.0002	0.0179	0.1445	1001.1^{ED}	7.6		
$^5S_2+{}^5F_4\rightarrow{}^5I_7$	765.1	0.0012	0.0274	0.2773	2584^{ED}	19.7		

$^5S_2+^5F_4 \rightarrow {}^5I_8$	549.0	0.0207	0.0197	0.0041	8946^{ED}	68.1

*‹λ› - mean wavelength of the emission band, $A^{\Sigma}_{calc}(JJ')$ – probability of radiative spontaneous transition, $B(JJ')$ – luminescence branching ratio, A_{tot} and τ_{rad} – total probability of radiative spontaneous transitions and the radiative lifetime of the excited state, respectively, $U^{(k)}$ – squared reduced matrix elements, ED and MD stand for the electric-dipole and magnetic-dipole contributions, respectively.

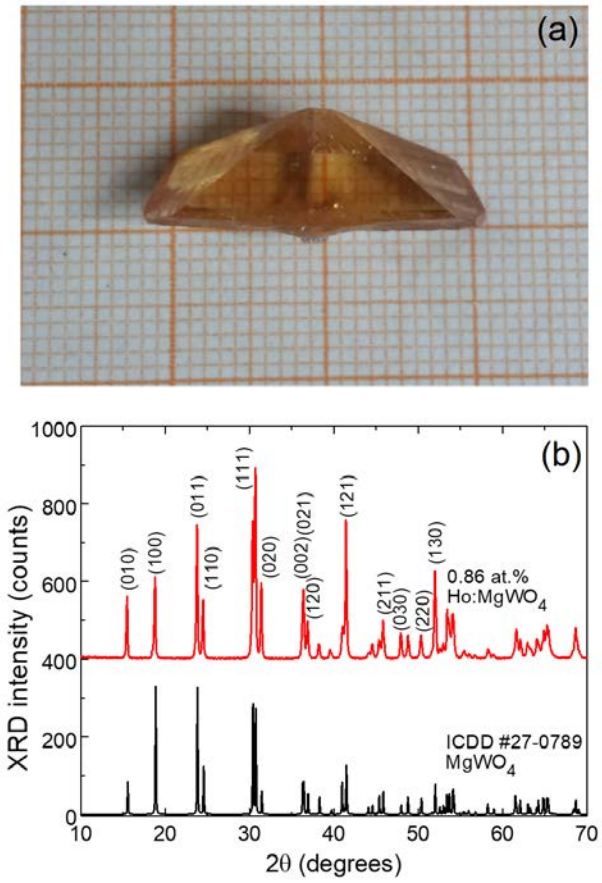

Fig. 1. (a) Photograph of the as-grown 0.86 at.% Ho^{3+}:$MgWO_4$ crystal (growth direction - along the [010] axis, the [100] axis is pointing towards the observer); (b) room-temperature X-ray powder diffraction (XRD) pattern of Ho^{3+}:$MgWO_4$ (in *red*) and a reference pattern of $MgWO_4$ (in *black*, ICDD card #27-0789), *numbers* denote the Miller's indices, (*hkl*).

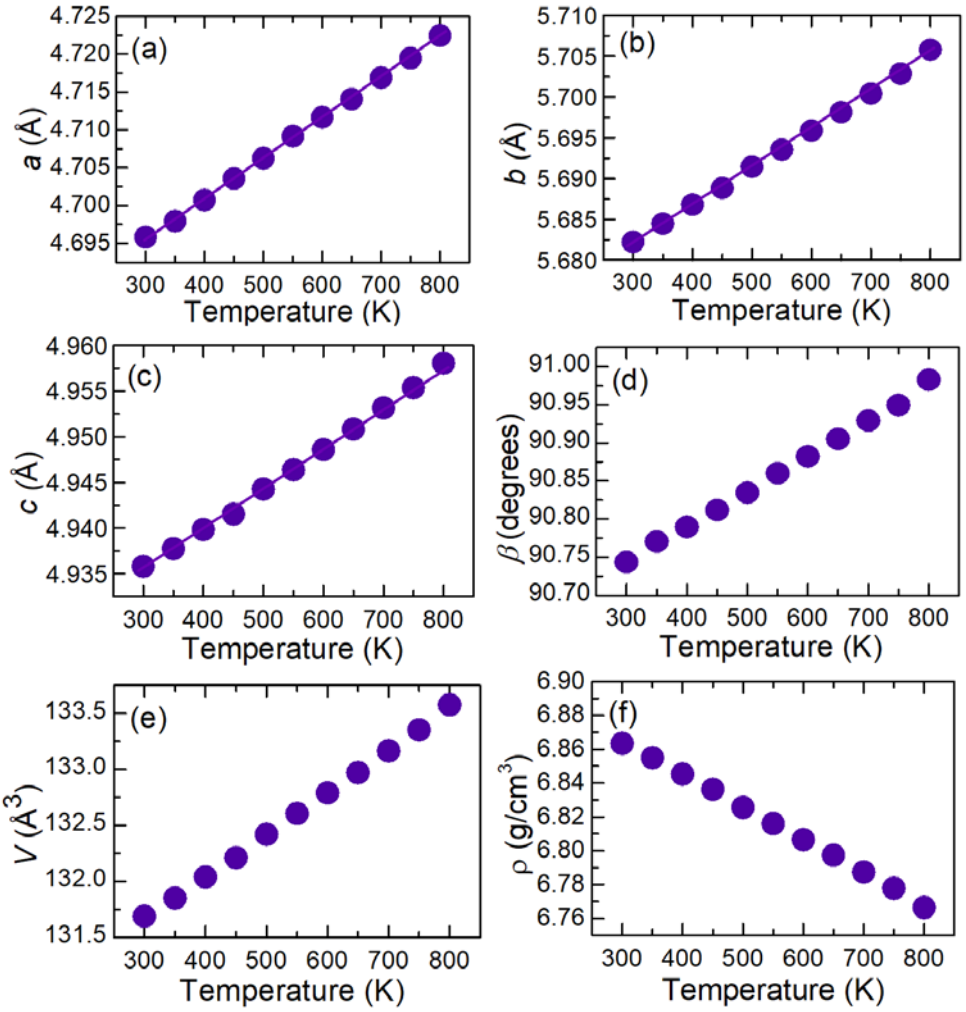

Fig. 2. (a-f) Dependence of lattice constants *a*, *b*, *c* and *β*, volume of the unit-cell *V* and calculated density ρ_{calc} of 0.86 at.% Ho^{3+}:$MgWO_4$ crystal on temperature: *symbols* – experimental data extracted from the XRD patterns, *lines* in (a-c) – their linear fits.

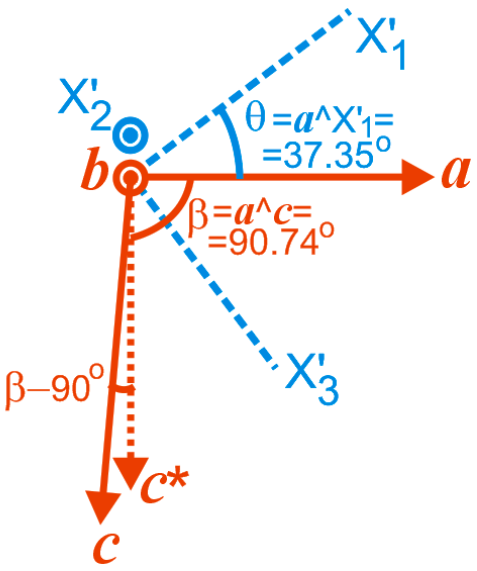

Fig. 3. Mutual orientation of the crystallographic axes (***a***, ***b***, ***c*** and ***c**** = ***a*** × ***b***) and principal axes of the thermal expansion tensor X'_k (k = 1, 2, 3) for the Ho^{3+}:$MgWO_4$ crystal.

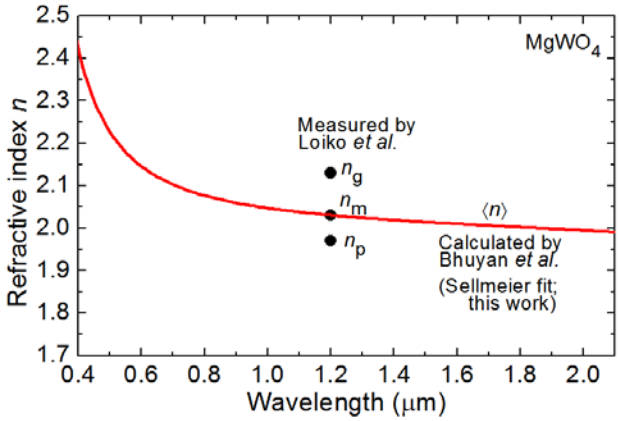

Fig. 4. Refractive index of $MgWO_4$: *red curve* – calculated dispersion of the mean refractive index ⟨*n*⟩ from Ref. [25], fitted using the two-pole Sellmeier equation, Eq. (2), *circles* – experimental data from Ref. [15].

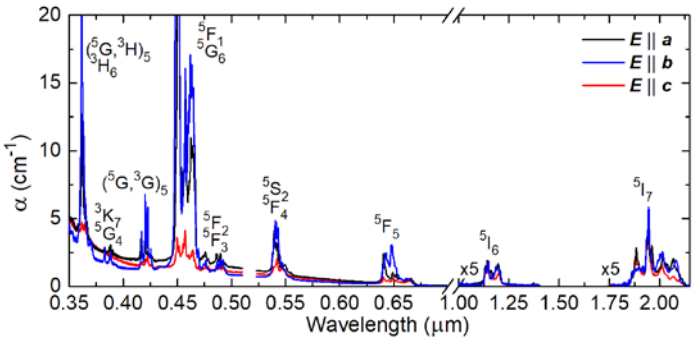

Fig. 5. Room-temperature absorption spectra of 0.86 at.% Ho^{3+}:$MgWO_4$ for light polarizations ***E*** || ***a***, ***b***, ***c***.

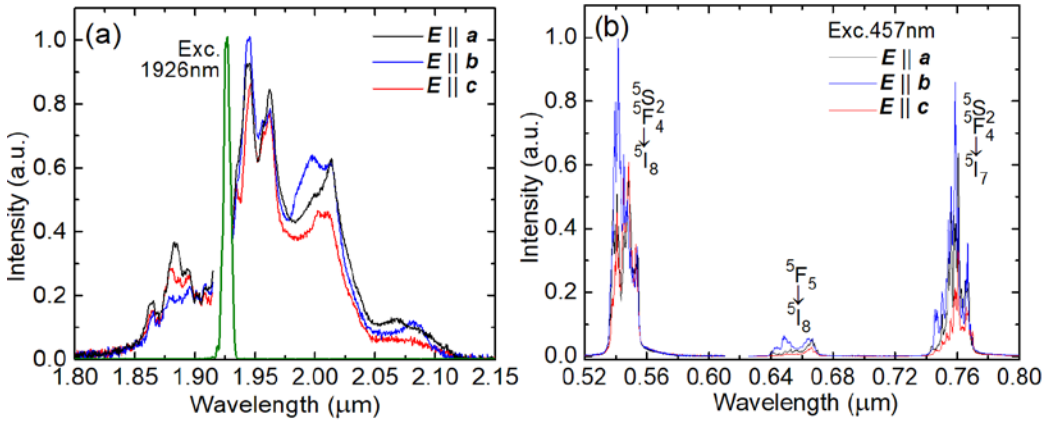

Fig. 6. Room-temperature emission spectra of Ho^{3+} in $MgWO_4$ in the near-IR (a) and in the visible (b) for light polarizations ***E*** || ***a***, ***b***, ***c***. The excitation wavelengths are λ_{exc} = 1926 nm (a) and 457 nm (b). Green spectrum in (a) – emission of the exciting laser diode.

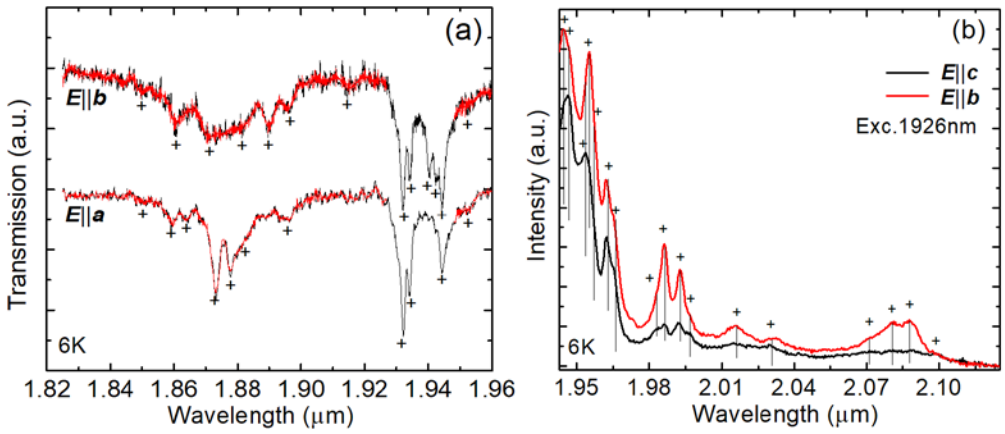

Fig. 7. Low-temperature (6 K) absorption (a) and luminescence (b) spectra of the $^5I_8 \leftrightarrow {}^5I_7$ transition of Ho^{3+} in $MgWO_4$. + indicates the peaks identified as Stark-to-Stark transitions. The light polarizations are ***E*** || ***a***, ***E*** || ***b*** (a) and ***E*** || ***b***, ***E*** || ***c*** (b). In (a), the *red curves* are after Fourier transform noise filtering. In (b), λ_{exc} = 1926 nm.

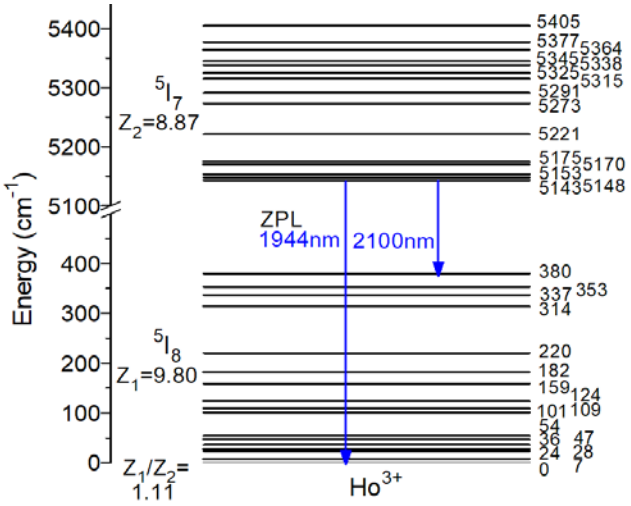

Fig. 8. Stark splitting of the ground-state ($^5I_8$) and the upper laser level ($^5I_7$) of Ho^{3+} in $MgWO_4$. *Numbers* denote the energies of Stark sub-levels in cm^{-1}. $Z_{1(2)}$ are the calculated partition functions, *arrows* indicate the ZPL transition and the transition corresponding to the longest emission wavelength.

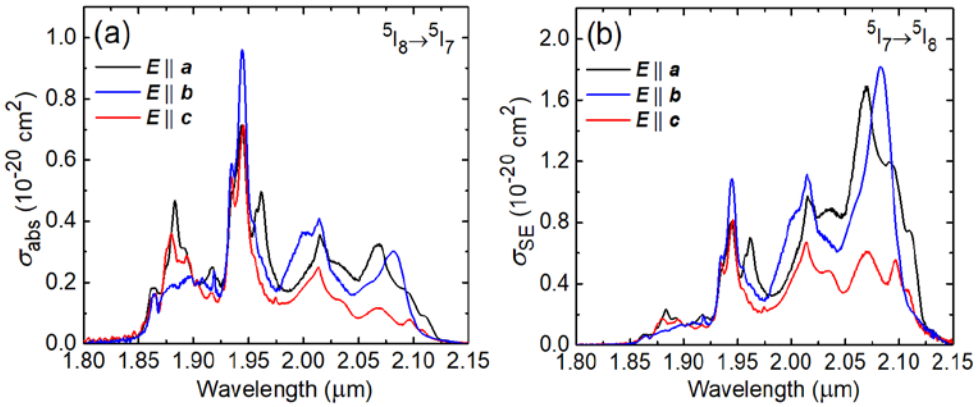

Fig. 9. (a) Room-temperature absorption, σ_{abs}, and (b) stimulated-emission, σ_{SE}, cross-sections for the $^5I_8 \leftrightarrow {}^5I_7$ transition of Ho^{3+} in $MgWO_4$. Light polarizations are $\boldsymbol{E} \parallel \boldsymbol{a}, \boldsymbol{b}, \boldsymbol{c}$. σ_{SE} values are calculated with the RM.

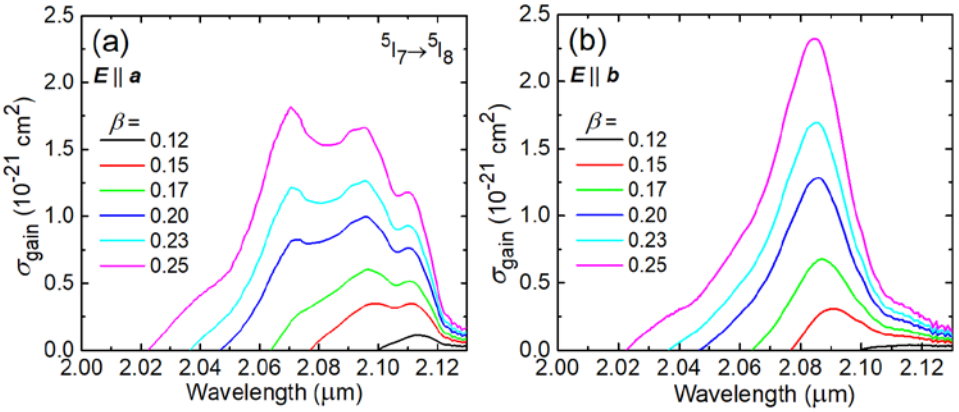

Fig. 10. Room-temperature gain cross-sections, $\sigma_{gain} = \beta\sigma_{SE} - (1-\beta)\sigma_{abs}$, for the $^5I_7 \rightarrow {}^5I_8$ transition of Ho^{3+} in $MgWO_4$ for various inversion ratios $\beta = N_2(^5I_7)/N_{Ho}$. Light polarizations are ***E*** || ***a*** (a) and ***E*** || ***b*** (b).

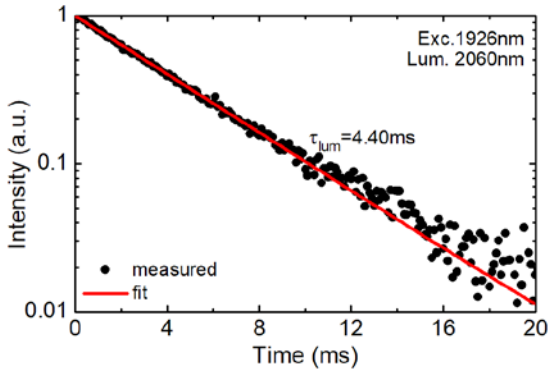

Fig. 11. Room-temperature luminescence decay curve for the 0.86 at.% Ho^{3+}:$MgWO_4$ crystal, *circles* – experimental data, *line* – single-exponential fit, λ_{exc} = 1926 nm, λ_{lum} = 2060 nm.

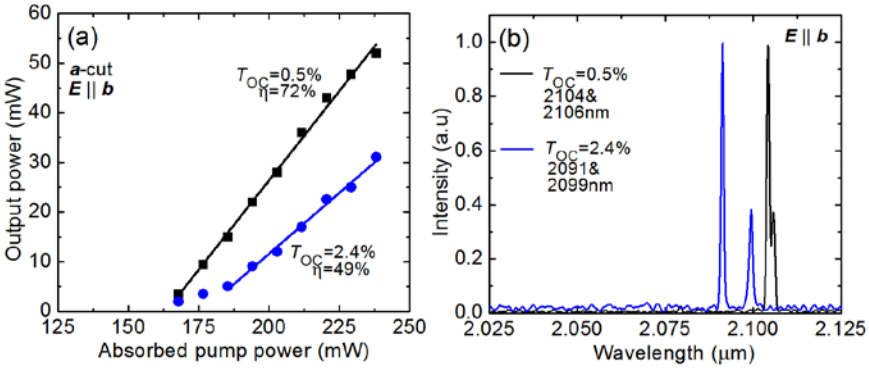

Fig. 12. In-band pumped ***a***-cut Ho^{3+}:$MgWO_4$ laser: (a) input-output dependences, η – slope efficiency; (b) typical laser emission spectra measured at P_{abs} = 240 mW. The laser polarization is ***E*** || N_m (***b***).